Volume 16, Issue 2, 162504 (1-14)

International Journal of Industrial Chemistry (IJIC)

https://doi.org/10.57647/j.ijic.2025.1604.19

Enhancing Carbon Dioxide Solubility and Interfacial Behavior in Saline Systems Using Diamine-Functionalized Silica Nanoparticles

Moslem Cheraghi [1], Mohammad Amin Gholamzadeh [2,*], Amin Azdarpour [3,*], Ali Borsalani [1], Mohammad Reza Asghari Ganjeh [4]

[1] *Department of Chemical Engineering, Om. C., Islamic Azad University, Omidiyeh, Iran*
[2] *Department of Petroleum Engineering, Om. C., Islamic Azad University, Omidiyeh, Iran*
[3] *Department of Petroleum Engineering, Marv. C., Islamic Azad University, Marvdasht, Iran*
[4] *Department of Chemistry, Om. C., Islamic Azad University, Omidiyeh, Iran*

[*] **Corresponding authors:** m.a.gholamzadeh@iau.ac.ir, aminazh22@gmail.com, amin.azdarpour@iau.ac.ir

Article History:

Received:
15 November 2025

Revised:
15 December 2025

Accepted:
30 December 2025

Published in Issue:
30 December 2025

Abstract

Understanding and enhancing carbon dioxide (CO_2) solubility and interfacial behavior in saline aqueous systems are critical for improving the efficiency of subsurface CO_2 sequestration and related applications. In this study, diamine-functionalized silica nanoparticles were synthesized using N-(2-aminoethyl)-3-aminopropyltrimethoxysilane (AEAPTMS) and systematically evaluated for their ability to enhance CO_2 solubility and reduce CO_2 –brine interfacial tension (IFT) under reservoir-relevant conditions. CO_2 solubility measurements were conducted in fresh water, formation brine (FB), and single-salt solutions with controlled ionic strength over a wide range of temperatures (25–80 °C) and pressures (up to 300 bar). The results show that the synthesized nanoparticles significantly enhance CO_2 solubility in both low- and high-salinity environments, with an optimal nanoparticle concentration of 2000 ppm. Despite the strong salting-out effect observed at elevated ionic strength, nanoparticle addition consistently mitigated salinity-induced solubility reduction. IFT measurements further confirmed that AEAPTMS-functionalized silica nanoparticles effectively reduce CO_2–brine IFT across all investigated pressures. The combined solubility and interfacial results demonstrate that surface-engineered silica nanoparticles provide a robust and effective strategy for improving CO_2 – aqueous phase interactions in complex brine systems. This work offers new mechanistic insights into nanoparticle-assisted CO_2 behavior and highlights the potential of chemically tailored nanomaterials for enhancing CO_2 storage performance in saline reservoirs.

Keywords: AEAPTMS-functionalized silica nanoparticles; CO_2 solubility; CO_2 sequestration; FB; IFT

Cite this article: Cheraghi M, Gholamzadeh M A, Azdarpour A, Borsalani A, Asghari Ganjeh M R. Enhancing Carbon Dioxide Solubility and Interfacial Behavior in Saline Systems Using Diamine-Functionalized Silica Nanoparticles. Int. J. Ind. Chem. 2025; 16(4): 1-14. https://doi.org/10.57647/j.ijic.2025.1604.19

1. Introduction

The continuous rise in atmospheric CO_2 concentration is one of the most critical drivers of global climate change and is largely attributed to the persistent reliance on fossil fuels for energy production and industrial activities. Since the pre-industrial era, global CO_2 levels have increased substantially, exceeding thresholds commonly associated with intensified global warming, more frequent extreme weather events, and long-term environmental instability. Although renewable energy technologies have expanded rapidly in recent years, fossil fuels are expected to remain a major component of the global energy mix for decades, particularly in hard-to-abate sectors such as power

generation, cement, steel, and petrochemical industries [1–6].

Within this context, carbon capture and storage (CCS) has emerged as a promising mitigation strategy with the potential to significantly reduce CO_2 emissions at their source. By capturing CO_2 from large point emitters and securely storing it in deep geological formations, CCS provides a technically feasible and scalable approach to decoupling industrial activity from greenhouse gas emissions. As a result, the development and optimization of CCS technologies are increasingly recognized as essential elements of comprehensive climate mitigation strategies aimed at limiting global temperature rise and achieving long-term carbon neutrality goals [7–11].

Geological storage of CO_2 in deep saline aquifers represents a viable approach for mitigating anthropogenic emissions and supporting the achievement of net-zero climate targets. The effectiveness of CO_2 storage in subsurface formations is governed by a combination of geochemical reactions and interfacial processes occurring within rock–CO_2–brine and CO_2–brine systems. Among these processes, the interfacial tension (IFT) between CO_2 and brine plays a critical role in controlling capillary sealing efficiency and, consequently, the achievable storage capacity. Accurate determination of CO_2–brine IFT under representative subsurface conditions, including pressure, temperature, salinity, and realistic brine composition, is therefore essential for reliable assessment of storage performance and containment integrity. In this work, new CO_2–brine IFT datasets are presented using the pendant drop technique over a pressure range of 0–20 MPa at temperatures of 298, 323, and 343 K. Measurements were conducted for three aqueous systems: fresh water, a 21.4 wt% NaCl brine, and a 21.4 wt% formation brine composed of mixed salts derived from a Middle Eastern reservoir.

A comprehensive analysis of the parameters influencing IFT is provided, together with a critical discussion of experimental factors affecting IFT measurements, including the role of CO_2–water equilibrium. For all investigated systems, IFT decreases monotonically with increasing pressure until reaching a plateau at approximately 12 MPa, beyond which it remains nearly constant at a characteristic pressure. In contrast, IFT consistently increases with temperature across the studied conditions. The minimum IFT value of 22.8 $mN \cdot m^{-1}$ was observed at 20 MPa and 298 K, while the maximum value of 78.92 $mN \cdot m^{-1}$ occurred at 0.1 MPa and 298 K. In addition, the presence of dissolved salts leads to higher IFT values, with divalent cations exerting a more pronounced effect than monovalent ions. Under identical salinity, pressure, and temperature conditions, CO_2/formation brine systems consistently exhibit higher IFT values than corresponding CO_2/NaCl brine systems. Furthermore, the influence of mixed salts on CO_2 saturation and storage capacity was evaluated through core-flooding experiments, which revealed CO_2 saturations of 38% in NaCl-saturated cores compared to 22% in formation-brine-saturated cores. Collectively, these results provide valuable experimental data and mechanistic insights into interfacial phenomena that are critical for the reliable design and assessment of subsurface CO_2 storage operations [12].

Recent studies have demonstrated that interpretable white-box models based on multigene genetic programming (MGGP) can accurately predict gas mixture solubility over wide ranges of pressure, temperature, and salinity. These models have achieved R^2 values of up to 0.9967 for CO_2 and 0.9914 for N_2, along with low RMSE values on the order of 10^{-4}–10^{-5}. When coupled with explainability tools such as SHAP analysis, MGGP-based models provide practical and physically interpretable solutions for CCS applications involving impure gas streams [13].

CO_2–brine–rock interactions play a fundamental role in controlling multiphase CO_2 flow and maintaining the integrity of subsurface storage formations. Despite their importance, the combined effects of brine salinity, rock mineralogy, and organic matter on CO_2 wettability at the nanoscale are not yet fully understood. To address this knowledge gap, molecular dynamics (MD) simulations have been employed to investigate key interfacial properties, including density distribution profiles and radial distribution functions (RDF, g(r)), in CO_2-saturated aqueous systems with high and low salinity. The simulation results indicate that mineralogical composition strongly governs CO_2 wettability behavior.

Specifically, reduced salinity promotes increased CO_2 wettability on siloxane surfaces, whereas aluminol surfaces exhibit the opposite trend. In addition, RDF analysis highlights the critical role of organic matter chemistry, showing that basic functional groups (–N) favor CO_2-wet conditions, while acidic groups (–COOH) promote water-wet behavior.

By jointly considering the effects of salinity, mineralogy, and organic matter, these findings provide valuable nanoscale insight into the mechanisms governing CO_2 wettability and offer a conceptual framework for mitigating leakage risks in geological CO_2 sequestration [14].

CO_2–brine–rock interactions exert a strong influence on reservoir properties, with distinct impacts observed in gas and water zones. Experimental studies conducted using core plugs, rock fragments, and formation brine from the DF gas field—a large aquifer-supported gas reservoir in the South China Sea—have shown that dissolved CO_2 forms carbonic acid in brine, which promotes mineral dissolution and particle detachment.

These processes can lead to permeability reduction, thereby impairing CO_2 injectivity and storage performance, with more pronounced formation damage occurring in gas-bearing zones. In contrast, high-quality reservoirs in water zones may experience enhanced porosity and permeability due to mineral dissolution, which can improve CO_2 storage potential. A combination of analytical techniques, including scanning electron microscopy (SEM), energy-dispersive spectroscopy (EDS), X-ray diffraction (XRD), and flame atomic absorption spectroscopy (FAAS), has been used to elucidate the mechanisms responsible for these petrophysical changes. Collectively, these findings indicate that preferential injection of dry CO_2 into appropriately selected aquifers can help mitigate adverse formation damage, providing practical guidance for the design and optimization of CO_2 injection and storage strategies in aquifer-supported gas reservoirs [15].

Despite extensive research on CO_2 solubility, interfacial tension, and CO_2–brine–rock interactions under geological storage conditions, existing studies largely focus on pressure–temperature effects, simplified brine compositions, or predictive modeling approaches. Far less attention has been given to active chemical strategies capable of directly modifying CO_2–aqueous phase interactions in high-salinity reservoir fluids, particularly through the use of engineered nanomaterials. Moreover, most nanoparticle-based investigations rely on physically dispersed or non-functionalized particles, offering limited control over molecular-level interactions with CO_2 and often exhibiting reduced effectiveness in complex formation brines.

To date, a systematic experimental assessment of surface-functionalized nanoparticles designed to enhance CO_2 solubility while simultaneously reducing CO_2–brine interfacial tension across a wide range of pressures, temperatures, salinities, and salt chemistries remains notably absent.

Addressing this gap, the present study introduces diamine-functionalized silica nanoparticles synthesized using N-(2-aminoethyl)-3-aminopropyltrimethoxysilane (AEAPTMS) as a chemically tailored platform to actively promote CO_2–aqueous phase affinity under reservoir-relevant conditions.

By integrating controlled nanoparticle synthesis with comprehensive solubility and interfacial measurements in fresh water, single-salt solutions, and realistic formation brines, this work provides new mechanistic insight into nanoparticle-assisted CO_2 behavior in complex saline systems. The findings establish a unified experimental framework that links nanoparticle surface chemistry to macroscopic CO_2 solubility and interfacial performance, offering a practical and scalable pathway for enhancing CO_2 storage efficiency in saline reservoirs.

2. Materials and Methods

2.1. Materials

In this study, FB with a total dissolved solids (TDS) content of 83,188 ppm was collected from one of the Iranian carbonate oil reservoirs. The ionic composition of the FB used in this work is summarized in Table 1. Analytical-grade salts, including $NaHCO_3$, Na_2CO_3, NaCl, KCl, Na_2SO_4, $CaCl_2$, $MgCl_2$, and $MgSO_4$, each with a purity of 99%, were purchased from local suppliers. Fresh water was also used for the preparation of salt solutions. The ionic strength of the FB was calculated to be approximately 1.55 $mol \cdot L^{-1}$ (1.55 M).

2.2. Synthesize of AEAPTMS-functionalized silica nanoparticles

The AEAPTMS-functionalized silica nanoparticles were synthesized through a controlled surface silanization approach designed to ensure uniform grafting of diamine groups while preserving nanoparticle dispersion. Initially, commercially available colloidal silica nanoparticles were dried under mild vacuum to remove physically adsorbed moisture and to activate surface silanol groups. The dried nanoparticles were then redispersed in anhydrous ethanol using ultrasonic agitation to obtain a homogeneous suspension. Separately, a measured amount of N-(2-aminoethyl)-3-aminopropyltrimethoxysilane was slowly introduced into the silica suspension under continuous stirring.

A small and controlled amount of deionized water was added to promote partial hydrolysis of the methoxy groups, enabling covalent bonding between the silane molecules and the surface silanol groups of silica. The reaction mixture was maintained under reflux at moderate temperature while being continuously stirred to allow sufficient time for condensation and surface grafting to occur.

Throughout this step, the reaction environment was kept mildly basic to prevent excessive silane self-polymerization and to favor surface-specific functionalization.

Table 1. Ion composition of the FB used in this study

Ion	Concentration (ppm)
Ca^{2+}	1184
Mg^{2+}	1944
Na^{+}	25392
HCO_3^{-}	45
SO_4^{2-}	1200
Cl^{-}	53423
TDS	83188

Upon completion of the reaction, the functionalized nanoparticles were separated by centrifugation and thoroughly washed with ethanol to remove any unreacted silane or physically adsorbed species.

The washed nanoparticles were then dried at low temperature under vacuum to preserve the integrity of the grafted diamine groups. This synthesis route yields uniformly functionalized AEAPTMS-silica nanoparticles with enhanced surface amine density and improved stability in aqueous and saline environments. The mild reaction conditions and solvent choice minimize particle aggregation and ensure that the resulting nanoparticles are suitable for interfacial and wettability studies under reservoir-relevant conditions.

Transmission electron microscopy (TEM) was employed to examine the morphology and primary size of the silica nanoparticles before and after surface functionalization, ensuring that the modification process did not alter particle structure or induce aggregation. Dynamic light scattering (DLS) was used to measure the hydrodynamic size distribution of the nanoparticles in aqueous suspension, where changes in particle size after functionalization served as an indirect indication of successful surface modification.

2.3 CO_2 solubility measurement

The solubility of CO_2 in fresh water and FB was measured using a high-pressure, high-temperature equilibrium system operating under a static–analytic approach, following a procedure adapted from previously reported methodologies. The experimental setup consisted of a 300 mL stainless-steel reactor (Parr Instruments) fitted with a temperature-regulated jacket, a magnetic stirring unit, a high-precision digital pressure sensor (±0.1 bar), and dedicated sampling ports for both gas and liquid phases. Before each experiment, the cell was thoroughly evacuated and purged several times with high-purity CO_2 to remove any residual air.

For each run, approximately 200 mL of the test solution was transferred into the reactor, and the temperature was stabilized at the target value (25–80 °C) using a thermostatically controlled oil bath with an accuracy of ±0.1 °C. Ultra-high-purity CO_2 (99.999%) was then injected incrementally until the desired pressure range (1–300 bar) was achieved. The system was continuously stirred at 400 rpm and allowed to equilibrate for 24 h. Equilibrium conditions were assumed once both pressure and temperature remained unchanged for a minimum duration of 30 min.

Upon reaching equilibrium, a small aliquot of the liquid phase was collected through a high-pressure sampling valve into a pre-weighed container, rapidly depressurized, and subsequently analyzed for total inorganic carbon using a Shimadzu TOC-L analyzer. CO_2 solubility, expressed in $mol \cdot kg^{-1}$, was calculated based on the measured TIC values and further verified through a carbon mass balance between the gas and liquid phases. Control experiments without nanoparticles were carried out under identical operating conditions to establish baseline solubility values at each temperature and pressure. Additional tests were performed using different concentrations of the synthesized nanoparticles dispersed in various solutions, and the corresponding CO_2 solubility was determined accordingly. A schematic illustration of the experimental apparatus used for CO_2 solubility and pH measurements is shown in Fig. 1(a).

2.4. IFT measurement

The IFT between CO_2 and FB was evaluated in both nanoparticle-free systems and in the presence of 2000 ppm of the synthesized nanoparticles using a high-pressure, high-temperature IFT-700 instrument as shown in Fig. 1(b). During each measurement, a droplet of brine was generated at the end of a finely calibrated capillary and exposed to the surrounding CO_2 phase inside a transparent high-pressure cell. Once the droplet shape became stable, the equilibrium IFT was calculated using axisymmetric drop shape analysis (ADSA).

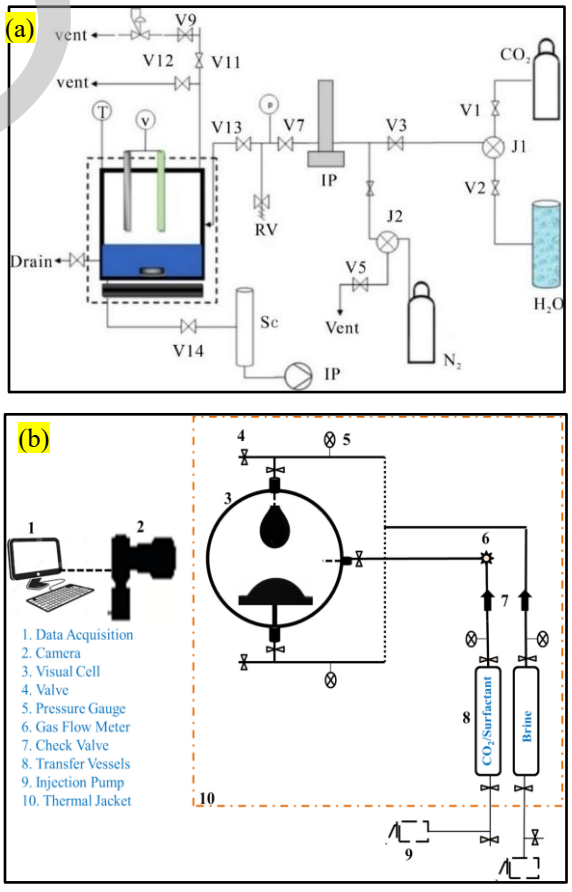

Figure 1. (a) CO_2 solubility measurement [16]; (b) IFT measurement [17]

Reliable determination of IFT required accurate density data for both phases under the applied experimental conditions. The density of pure CO_2 at the specified pressures and temperature was obtained from the physical properties data service thermophysical property database. In contrast, the densities of the FB and nanoparticle-dispersed brine were measured experimentally using the HPHT visual cell by relating the injected fluid mass to the precisely known cell volume. All IFT measurements were carried out at a temperature of 80 °C and pressures of up to 300 bar to closely replicate reservoir conditions and to maintain consistency with the CO_2 solubility and pH measurements performed in this study.

2.5. Preparation of single salts with constant ionic strength

To prepare single-salt solutions matching the ionic strength of the FB (approximately 1.55 M), the appropriate amounts of each salt were dissolved in deionized water under constant stirring at room temperature until fully dissolved. For monovalent salts such as NaCl, KCl, and $NaHCO_3$, a concentration of 1.55 M was used to achieve the target ionic strength. For salts containing divalent ions, including $CaCl_2$, $MgCl_2$, Na_2CO_3, and Na_2SO_4, the solutions were prepared at a slightly lower concentration of 0.517 M to account for their higher charge contribution. $MgSO_4$, which contains two divalent ions, was prepared at a concentration of 0.388 M. All solutions were stirred until clear and homogeneous, ensuring complete dissolution, and were stored in clean, sealed containers to prevent evaporation or contamination. These standardized single-salt solutions were then used for evaluating nanoparticle stability, CO_2 solubility, and interfacial properties under conditions that mimic the FB environment.

3. Results and Discussions

3.1. Characterization of synthesized AEAPTMS-functionalized SiO_2 nanoparticles

Fig. 2(a) shows the TEM image of the pristine SiO_2 nanoparticles, while Fig. 2(b) presents the TEM image of the AEAPTMS-functionalized SiO_2 nanoparticles. As observed in these micrographs, surface functionalization does not lead to any noticeable change in the primary particle size or morphology, indicating that the silanization process occurs as a surface modification rather than through particle growth or aggregation. In contrast, dynamic light scattering (DLS) measurements reveal a clear increase in the hydrodynamic diameter of the nanoparticles after functionalization. As shown in Figs. 2(c) and 2(d), the average hydrodynamic size increases from 135 nm for bare SiO_2 nanoparticles to 143 nm for AEAPTMS-functionalized SiO_2 nanoparticles when dispersed in water. This increase is attributed to the presence of the grafted AEAPTMS layer on the nanoparticle surface, which contributes to an expanded hydration shell and enhanced interaction with surrounding water molecules. Additionally, the introduction of diamine functional groups increases surface polarity and electrostatic interactions, leading to a thicker effective solvation layer in aqueous media. The combined TEM and DLS results confirm successful surface functionalization of the silica nanoparticles without inducing particle agglomeration. While TEM reflects the unchanged solid core size, DLS captures the influence of surface chemistry on nanoparticle behavior in suspension. This distinction is particularly important for applications involving interfacial phenomena and CO_2–brine systems, as the hydrodynamic size governs nanoparticle transport, stability, and interfacial activity under reservoir-relevant conditions [9–11,18–22].

3.2. CO_2 solubility in the absence of nano-particle

Fig. 3 illustrates the variation of CO_2 solubility in fresh water as a function of temperature and pressure. The results clearly show that temperature has a pronounced effect on CO_2 solubility, with lower temperatures favoring higher solubility. As the temperature increases from 25 to 80 °C, CO_2 solubility decreases significantly, reaching its maximum value at 25 °C and its minimum at 80 °C. This behavior is consistent with the exothermic nature of gas dissolution in liquids, where increased thermal energy at higher temperatures reduces gas–liquid affinity. In addition, CO_2 pressure strongly influences solubility, with higher pressures leading to increased dissolution due to enhanced gas fugacity.

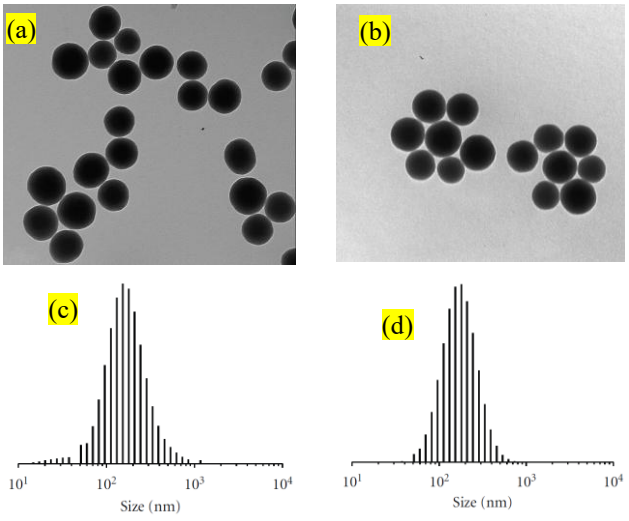

Figure 2. TEM image of (a) SiO_2, (b) AEAPTMS-functionalized SiO_2, and size distributions measured by DLS for (c) SiO_2 (135 nm), (d) AEAPTMS-functionalized SiO2 (143 nm)

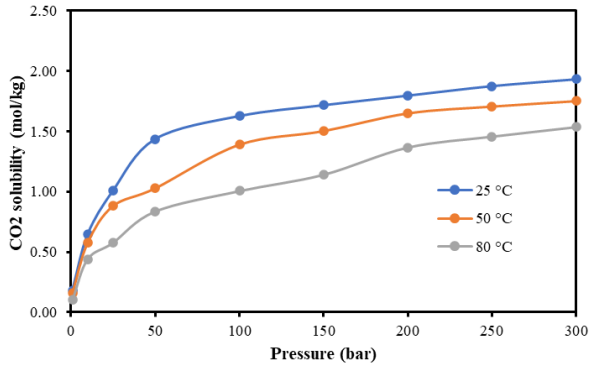

Figure 3. CO_2 solubility in fresh water at different temperatures in the absence of nano particle

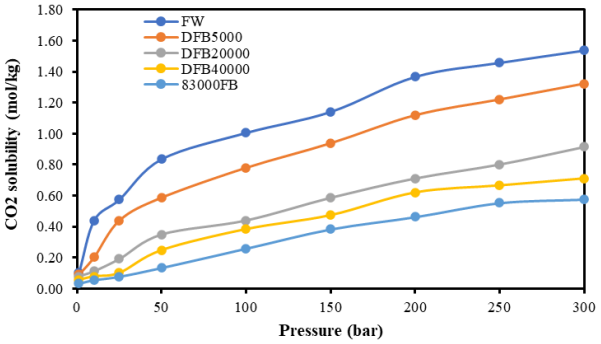

Figure 4. CO_2 solubility in different brines at 80 °C in the absence of nano particle

At a CO_2 pressure of 300 bar, the measured solubility values are 1.93, 1.75, and 1.55 mol·kg^{-1} at 25, 50, and 80 °C, respectively, confirming the combined effects of pressure enhancement and temperature suppression on CO_2 solubility. Fig. 4 presents CO_2 solubility data obtained at 80 °C under varying CO_2 pressures for brines with different salinities. The results demonstrate a clear inverse relationship between brine salinity and CO_2 solubility. As salinity increases, CO_2 solubility systematically decreases, reflecting the well-known salting-out effect, whereby dissolved ions reduce the availability of free water molecules for gas dissolution. At a CO_2 pressure of 300 bar, CO_2 solubility values decrease from 1.54 mol·kg^{-1} in fresh water to 1.32, 0.92, 0.71, and 0.58 mol·kg^{-1} in DFB5000, DFB20000, DFB40000, and FB with a TDS of 83,000 ppm, respectively. These results highlight the significant impact of ionic strength and salinity on CO_2 solubility and underscore the challenging conditions encountered in high-salinity reservoir environments, providing a critical baseline for evaluating the effectiveness of nanoparticle-assisted CO_2 solubility enhancement. The observed trends in CO_2 solubility in fresh water and brine systems can be explained by the combined thermodynamic effects of temperature, pressure, and ionic strength. As shown in Fig. 3, decreasing temperature results in a pronounced increase in CO_2 solubility. This behavior is attributed to the exothermic nature of CO_2 dissolution in aqueous media, where lower temperatures favor gas–liquid interactions and reduce the kinetic energy of dissolved CO_2 molecules, thereby enhancing their retention in the liquid phase. At higher temperatures, increased molecular motion weakens these interactions, leading to a reduction in solubility [13,23–25]. Pressure exerts a strong and monotonic influence on CO_2 solubility across all investigated temperatures. Increasing CO_2 pressure from 1 to 300 bar increases the driving force for gas dissolution by elevating CO_2 fugacity, which enhances the mass transfer of CO_2 into the aqueous phase. The combined effects of high pressure and low temperature explain the maximum solubility observed at 25 °C and 300 bar. These trends are consistent with fundamental gas solubility behavior in aqueous systems under high-pressure conditions. The results presented in Fig. 4 further demonstrate the significant role of brine salinity in controlling CO_2 solubility. At a constant temperature of 80 °C, increasing salinity leads to a systematic decrease in CO_2 solubility across the entire pressure range. This reduction is primarily associated with the salting-out effect, whereby dissolved ions compete with CO_2 for hydration water molecules, effectively reducing the solvent capacity of the aqueous phase. Higher ionic strength also increases the activity coefficient of dissolved CO_2, making its dissolution thermodynamically less favorable [26–28].

In highly saline systems such as FB, the presence of both monovalent and divalent ions further intensifies this effect through strong electrostatic interactions and structured hydration shells, which limit the availability of free water molecules for CO_2 solvation. As a result, the lowest CO_2 solubility values are observed in the FB with a TDS of approximately 83,000 ppm. These findings highlight the severe limitations imposed by high salinity on CO_2 dissolution under reservoir conditions and emphasize the necessity of mitigation strategies, such as nanoparticle-assisted approaches, to overcome salinity-induced solubility reduction. Overall, the results from Figs. 3 and 4 establish a robust baseline for understanding CO_2 behavior in aqueous systems and provide critical context for evaluating the role of AEAPTMS-functionalized silica nanoparticles in enhancing CO_2 solubility under challenging reservoir-relevant conditions.

3.3. CO_2 solubility in the presence of nano-particles

Fig. 5 presents CO_2 solubility values in fresh water and FB at 80 °C and a CO_2 pressure of 300 bar for different nanoparticle concentrations. As shown in this figure, CO_2 solubility in fresh water is consistently higher than that in FB. In addition, increasing the nanoparticle concentration from 100 to 5000 ppm markedly enhances CO_2 solubility in both fresh water and FB. However, the increase in CO_2

solubility is pronounced when the nanoparticle concentration rises from 100 to 2000 ppm, while further increases from 2000 to 5000 ppm result in only marginal improvements. These results indicate that 2000 ppm represents an optimal nanoparticle concentration for enhancing CO_2 solubility. At this concentration, CO_2 solubility in fresh water and FB reaches 2.07 and 0.89 mol·kg^{-1}, respectively. Fig. 6 shows CO_2 solubility values in fresh water at different temperatures in the presence of 2000 ppm nanoparticles. As illustrated in this figure, the addition of 2000 ppm nanoparticles significantly enhance CO_2 solubility in fresh water across all investigated conditions. Moreover, increasing CO_2 pressure from 1 to 300 bar and decreasing temperature from 80 to 25 °C both contribute to improved CO_2 solubility. At a CO_2 pressure of 300 bar, CO_2 solubility in fresh water in the presence of 2000 ppm nanoparticles is 2.77, 2.54, and 2.34 mol·kg^{-1} at 25, 50, and 80 °C, respectively. Fig. 7 presents CO_2 solubility values in different brines at 80 °C in the presence of 2000 ppm nanoparticles. The results demonstrate that nanoparticle addition effectively enhances CO_2 solubility across all brine systems. Furthermore, decreasing brine salinity leads to higher CO_2 solubility, regardless of the applied pressure. At a CO_2 pressure of 300 bar, CO_2 solubility values of 2.07, 1.53, 1.08, 0.95, and 0.89 mol·kg^{-1} are obtained for fresh water, DFB5000, DFB20000, DFB40000, and FB, respectively. The enhancement of CO_2 solubility observed in Figs. 5–7 can be primarily attributed to the surface chemistry and interfacial activity of the AEAPTMS-functionalized silica nanoparticles. The presence of diamine functional groups on the nanoparticle surface introduces multiple active sites capable of interacting with dissolved CO_2 molecules through a combination of weak chemical interactions, such as reversible amine–CO_2 associations, and physical adsorption. These interactions increase the effective affinity of the aqueous phase toward CO_2, thereby promoting higher solubility [29–32]. As shown in Fig. 5, increasing nanoparticle concentration leads to a substantial increase in CO_2 solubility in both fresh water and FB. At low nanoparticle concentrations, the addition of nanoparticles significantly increases the available interfacial area and the number of active surface sites for CO_2 interaction, resulting in a sharp rise in solubility. However, beyond a certain concentration threshold, the system approaches interfacial and bulk saturation, where most accessible interfaces and interaction sites are already occupied. Consequently, further increases in nanoparticle concentration yield diminishing returns, explaining the relatively minor improvement in CO_2 solubility observed between 2000 and 5000 ppm. This behavior supports the identification of 2000 ppm as an optimal nanoparticle concentration for efficient CO_2 solubility enhancement. The results presented in Fig. 6 demonstrate that the beneficial effect of AEAPTMS-functionalized silica nanoparticles persists across a wide range of temperatures and pressures. While increasing pressure enhances CO_2 solubility by increasing gas fugacity and the thermodynamic driving force for dissolution, the nanoparticles further amplify this effect by stabilizing dissolved CO_2 within the aqueous phase. Similarly, although higher temperatures generally reduce CO_2 solubility due to decreased gas–liquid affinity, the presence of nanoparticles partially counteracts this effect by providing additional interaction pathways for CO_2 molecules. This indicates that the nanoparticles not only facilitate CO_2 transfer into the liquid phase but also retard its release at elevated temperatures, maintaining enhanced solubility under reservoir-relevant conditions [33–36]. Fig. 7 highlights the influence of brine salinity on nanoparticle-assisted CO_2 solubility. Increasing salinity inherently reduces CO_2 solubility due to the salting-out effect, in which dissolved ions compete with CO_2 for hydration water molecules and increase the activity coefficient of dissolved gas. Despite this limitation, the addition of AEAPTMS-functionalized silica nanoparticles significantly improves CO_2 solubility across all salinity levels. This suggests that the nanoparticles modify the local aqueous environment by creating micro-domains with enhanced CO_2 affinity and by partially shielding CO_2 molecules from direct ionic interactions. The effectiveness of the nanoparticles even in highly saline FB demonstrates their strong tolerance to high ionic strength and their ability to mitigate salinity-induced solubility reduction [37–39].

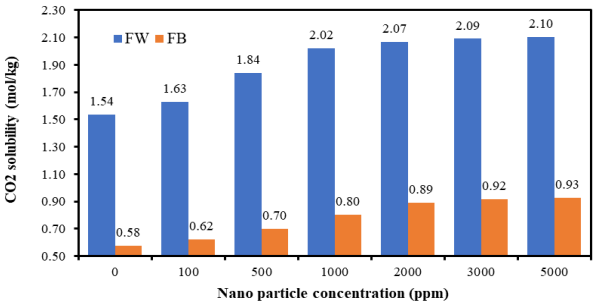

Figure 5. CO_2 solubility in fresh water and FB with different concentrations of nano particle at 80 °C and 300 bar CO_2 pressure

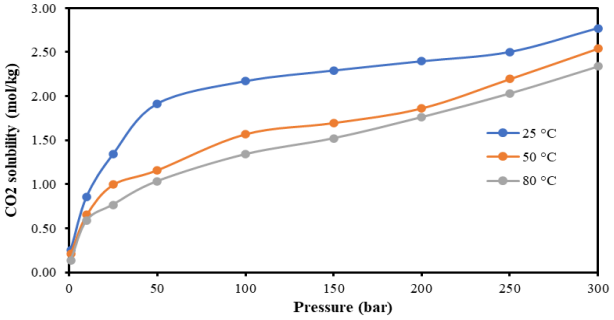

Figure 6. CO_2 solubility in fresh water at different temperatures in the presence of 2000 ppm nano particle

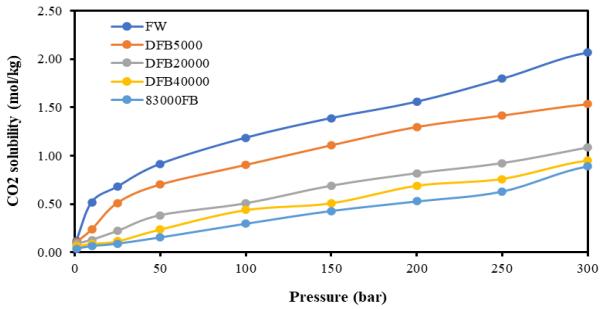

Figure 7. CO_2 solubility in different brines at 80 °C in the presence of 2000 ppm nano particle

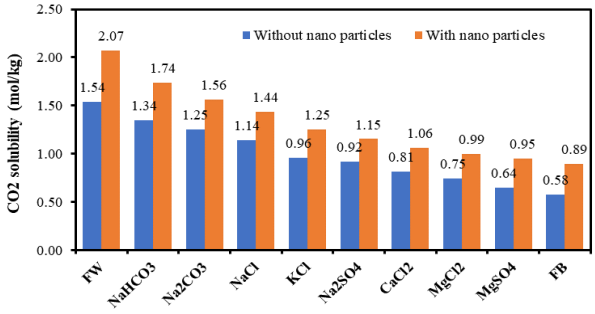

Figure 8. CO_2 solubility in different salt at 80 °C and 300 bar CO_2 pressure in the absence and presence of 2000 ppm nano particle

Overall, the combined results of Figs. 5–7 confirm that AEAPTMS-functionalized silica nanoparticles enhance CO_2 solubility through synergistic interfacial adsorption, increased effective gas–liquid contact area, and amine-mediated interactions. The persistence of these effects across varying temperatures, pressures, and salinities underscores the robustness of the nanoparticle design and highlights its potential applicability for CO_2 utilization and storage in realistic reservoir environments.

3.4. Effect of different types of salts on CO_2 solubility

Fig. 8 presents CO_2 solubility values in different salt solutions at 80 °C and 300 bar CO_2 pressure, both in the absence and presence of 2000 ppm nanoparticles. As shown in this figure, different salt types result in distinct CO_2 solubility values. In all cases, the addition of 2000 ppm nanoparticles significantly enhance CO_2 solubility. Among the investigated salts, $NaHCO_3$ exhibits the highest CO_2 solubility, reaching 1.74 and 1.34 mol·kg^{-1} in the presence and absence of 2000 ppm nanoparticles, respectively. In contrast, $MgSO_4$ shows the lowest CO_2 solubility, with values of 0.95 and 0.64 mol·kg^{-1} in the presence and absence of 2000 ppm nanoparticles, respectively. The variation in CO_2 solubility observed among different salt solutions in Fig. 8 can be attributed to differences in ionic composition, ion valency, and specific ion–water–CO_2 interactions. Salts containing monovalent ions, such as $NaHCO_3$, generally exhibit a weaker salting-out effect compared to salts with divalent ions. Monovalent ions disrupt the hydrogen-bonding network of water to a lesser extent, thereby preserving a higher capacity for CO_2 hydration and dissolution. The superior performance of $NaHCO_3$ can also be explained by the presence of bicarbonate ions, which participate directly in the carbonate equilibrium system. Bicarbonate ions facilitate the conversion of dissolved CO_2 into aqueous carbonate species, effectively shifting the equilibrium toward greater overall CO_2 uptake. This buffering capacity enhances apparent CO_2 solubility and makes $NaHCO_3$-based solutions particularly favorable for CO_2 dissolution under high-pressure conditions [24,40,41]. In contrast, $MgSO_4$ exhibits the lowest CO_2 solubility due to the strong salting-out effect associated with divalent cations and anions. Mg^{2+} ions possess a high charge density and strong hydration shell, which significantly reduces the availability of free water molecules for CO_2 solvation. Similarly, SO_4^{2-} ions further intensify ion–water interactions, collectively leading to a pronounced reduction in CO_2 solubility. The consistent enhancement in CO_2 solubility observed upon the addition of 2000 ppm AEAPTMS-functionalized silica nanoparticles across all salt systems highlights the robustness of the nanoparticle mechanism. The amine-functionalized nanoparticle surfaces provide additional interaction sites for CO_2 through reversible amine–CO_2 interactions and physical adsorption, partially offsetting the salting-out effects imposed by dissolved ions. Moreover, the nanoparticles likely alter the local microenvironment of the aqueous phase, creating regions with enhanced CO_2 affinity even in highly saline or divalent-ion-rich systems [27,42–44]. Overall, the results presented in Fig. 8 demonstrate that both salt type and nanoparticle functionalization play critical roles in controlling CO_2 solubility. While divalent salts impose stronger thermodynamic limitations on CO_2 dissolution, the incorporation of AEAPTMS-functionalized silica nanoparticles effectively mitigates these effects, underscoring their potential for application in complex, high-salinity reservoir fluids.

3.5. Effect of nano particle on IFT of CO_2 and FB

Table 2 presents the IFT values between CO_2 and FB in the absence and presence of 2000 ppm nanoparticles at 80 °C. In addition, the drop shapes of CO2 in the presence of nano particle is also shown in this table. As shown in this table, the addition of 2000 ppm nanoparticles results in a noticeable reduction in IFT between CO_2 and FB at all investigated pressures. In addition, increasing CO_2 pressure from 1 to 300 bar leads to a further decrease in IFT values. At a CO_2 pressure of 100 bar, the IFT between CO_2 and FB decreases from 35.66 mN·m^{-1} in the absence of nanoparticles to 24.21 mN·m^{-1} in the presence of 2000 ppm nanoparticles.

Table 2. Drop images and IFT values between CO_2 and FB in the presence and absence of 2000 ppm nano particles at 80 °C

P (bar)	IFT of CO_2 and FB in the absence of nano particles (mN/m)	IFT of CO_2 and FB in the presence of nano particles (mN/m)	Drop images of CO_2 in FB in the presence of nano particles
1	57.94	40.26	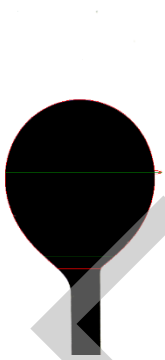
25	47.27	31.71	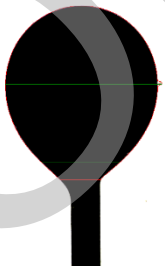
50	41.60	27.60	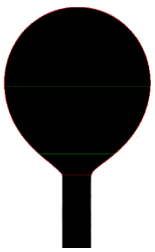
100	35.66	24.21	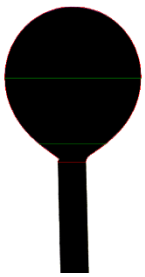

P (bar)	IFT of CO2 and FB in the absence of nano particles (mN/m)	IFT of CO2 and FB in the presence of nano particles (mN/m)	Drop images of CO2 in FB in the presence of nanoparticles
150	33.35	19.97	
200	29.71	17.58	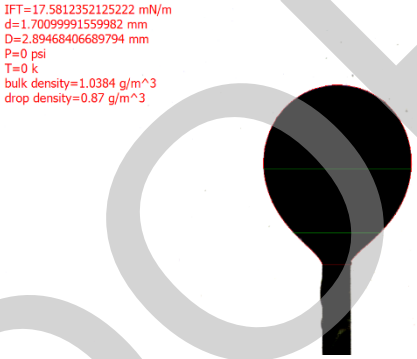
250	25.05	15.21	
300	23.02	10.84	

These values are further reduced to 23.02 and 10.84 $mN \cdot m^{-1}$, respectively, when the CO_2 pressure is increased to 300 bar.

The reduction in IFT observed in Table 2 can be attributed to the combined effects of elevated CO_2 pressure and the interfacial activity of AEAPTMS-functionalized silica nanoparticles. Increasing CO_2 pressure enhances the density of the CO_2 phase and promotes greater mutual affinity between CO_2 and the aqueous phase, which inherently lowers the interfacial free energy and results in reduced IFT values. The presence of AEAPTMS-functionalized silica nanoparticles further amplifies this effect by modifying the CO_2–brine interface. Due to their amphiphilic nature,

the nanoparticles preferentially migrate toward the fluid–fluid interface, where they adsorb and form a stabilizing interfacial layer. The amine functional groups on the nanoparticle surface interact favorably with CO_2 molecules, while the hydrophilic silica backbone remains well-dispersed in the aqueous phase. This dual affinity reduces the interfacial free energy and leads to a pronounced decrease in IFT [45–47].

The stronger IFT reduction observed at higher pressures suggests a synergistic interaction between pressure-induced CO_2 densification and nanoparticle adsorption. At elevated pressures, the increased solubility of CO_2 enhances its interaction with the amine-functionalized surfaces, facilitating more effective nanoparticle packing at the interface and further suppressing IFT. The substantial IFT reduction achieved in the presence of nanoparticles, particularly at high CO_2 pressures, is of practical significance for subsurface CO_2 -related applications. Lower IFT values improve CO_2 mobility, enhance capillary-driven displacement efficiency, and facilitate improved contact between CO_2 and formation fluids. These effects are especially relevant for CO_2 sequestration and enhanced oil recovery processes in high-pressure carbonate reservoirs, where interfacial phenomena play a critical role in governing fluid flow and trapping mechanisms [48–50]. Overall, the results presented in Table 2 confirm that AEAPTMS-functionalized silica nanoparticles are highly effective in reducing CO_2–brine IFT under reservoir-relevant conditions, complementing their positive impact on CO_2 solubility and reinforcing their potential for practical field applications.

4. Conclusion

This study demonstrates the effectiveness of synthesized AEAPTMS-functionalized silica nanoparticles in enhancing CO_2 solubility and reducing CO_2–brine IFT under conditions representative of subsurface reservoirs. The results confirm that CO_2 solubility decreases with increasing temperature and brine salinity, while increasing pressure enhances dissolution, consistent with established thermodynamic behavior. However, the introduction of diamine-functionalized nanoparticles significantly modifies these trends by increasing CO_2 affinity in both fresh water and highly saline FB.

Nanoparticle concentration was found to play a critical role, with a sharp increase in CO_2 solubility observed up to 2000 ppm, beyond which further additions resulted in only marginal improvements. This behavior indicates an optimal nanoparticle loading, balancing performance enhancement and material efficiency. The nanoparticles also proved effective across a wide range of salt types and ionic strengths, partially counteracting the salting-out effect, particularly in systems dominated by divalent ions.

IFT measurements revealed that AEAPTMS-functionalized silica nanoparticles substantially reduce CO_2–brine IFT, an effect that becomes more pronounced at higher pressures. This reduction is attributed to nanoparticle adsorption at the fluid–fluid interface and favorable amine–CO_2 interactions, which together lower interfacial free energy.

The results of this study have direct practical implications for subsurface CO_2 storage and related applications. The demonstrated ability of AEAPTMS-functionalized silica nanoparticles to simultaneously enhance CO_2 solubility and reduce CO_2–brine interfacial tension under high-pressure, high-temperature, and high-salinity conditions suggests their potential use as functional additives in CO_2 injection operations. By increasing CO_2 dissolution and improving interfacial characteristics, these nanoparticles may contribute to improved injectivity, enhanced storage efficiency, and more favorable trapping behavior in saline reservoirs. From an operational perspective, the identification of an optimal nanoparticle concentration provides a practical guideline for minimizing material usage while maximizing performance. Future work should focus on evaluating nanoparticle transport and stability in porous media, assessing long-term interactions with reservoir rocks, and extending the approach to dynamic flow conditions and field-scale scenarios. Such efforts will be essential for translating nanoparticle-assisted CO_2 management strategies from laboratory studies to practical deployment in geological storage projects.

Authors Contribution

All the authors have participated sufficiently in the intellectual content, conception and design of this work or the analysis and interpretation of the data (when applicable), as well as the writing of the manuscript.

Availability of data and materials

The data that support the findings of this study are available from the corresponding author, upon reasonable request.

Conflict of interests

The authors declare that they have no known competing financial interests or personal relationships that could have appeared to influence the work reported in this paper.

References

[1] Azimi N, Gandomkar A, Sharif M,. Relationship between production condition, microstructure and final properties of chitosan/graphene oxide–zinc oxide bionanocomposite, Polym Bull 2023;80:6455–69. https://doi.org/10.1007/s00289-022-04277-0

[2] Gandomkar A, Torabi F, Nasriani H R, Enick R M. Maximising CO2 sequestration efficiency in deep saline aquifers through in-situ generation of CO2-in-brine foam incorporating novel CO2-soluble non-ionic surfactants, Chemical Engineering Journal 2025;521:166102. https://doi.org/10.1016/j.cej.2025.166102

[3] Gandomkar A, Honarvar B, Kazemzadeh Y, Derikvand Z, An Experimental Study of Surfactant Alternating CO2 Injection for Enhanced Oil Recovery of Carbonated Reservoir, Iranian Journal of Oil and Gas Science and Technology 2016;5:1–17. https://doi.org/10.22050/ijogst.2016.41564

[4] Azdarpour A, Asadullah M, Mohammadian E, Junin R, Hamidi H, Manan M, Daud A R M, Mineral carbonation of red gypsum via pH-swing process: Effect of CO2 pressure on the efficiency and products characteristics, Chemical Engineering Journal. 2015; 264: 425–436. https://doi.org/10.1016/j.cej.2014.11.125

[5] Azdarpour A, Asadullah M, Junin R, Mohammadian E, Hamidi H, Daud A R M, Manan M, Extraction of calcium from red gypsum for calcium carbonate production, Fuel Processing Technology. 2015; 130: 12–19. https://doi.org/10.1016/j.fuproc.2014.09.034

[6] Azdarpour A, Asadullah M, Mohammadian E, Hamidi H, Junin R, Karaei M A, A review on carbon dioxide mineral carbonation through pH-swing process, Chemical Engineering Journal . 2015; 279: 615–630. https://doi.org/10.1016/j.cej.2015.05.064

[7] Villa R, Nieto S, Donaire A, Lozano P, Direct Biocatalytic Processes for CO2 Capture as a Green Tool to Produce Value-Added Chemicals, Molecules. 2023; 28:5520. https://doi.org/10.3390/molecules28145520

[8] Sharma G, Dwivedi K, Bafana A, Pakade Y, OICC Author R B. Wet air oxidation of leachate containing emulsified and solubilized hydrocarbons from crude oil-contaminated soil, Int. J. Ind. Chem. 2023; 10. https://doi.org/10.1007/s40090-019-0187-2

[9] Rajan K P, Gopanna A, Theravalappil R, Thomas S P. Systematic design, implementation and studentsâ perceptions of a Polymer Engineering course for Chemical Engineering curricula, International Journal of Industrial Chemistry. 2024; 15. https://doi.org/10.57647/j.ijic.2024.1501.04

[10] Mohammadpour A, Mirzaei M, Azimi A, Ghomsheh S M T. Solubility and absorption rate of CO2 in MEA in the presence of graphene oxide nanoparticle and sodium dodecyl sulfate, International Journal of Industrial Chemistry. 2019; 10. https://doi.org/10.1007/s40090-019-0184-5

[11] Haroun A A, Kamel S, Elnahrawy A M, Hammad A A, Hamadneh I, Al-Dujaili A H. Polyacetal/graphene/polypyrrole and cobalt nanoparticles electroconducting composites, International Journal of Industrial Chemistry. 2020; 11. https://doi.org/10.1007/s40090-020-00218-w

[12] Mouallem J, Arif M, Isah A, Raza A, Motiur Rahman M, Mahmoud M, Shahzad Kamal M, Effect of formation brine on interfacial interaction: Implications for CO2 storage, Fuel. 2024; 371: 131986. https://doi.org/10.1016/j.fuel.2024.131986

[13] Alatefi S., Amar M.N., Agwu O.E., Alkouh A., Toward explicit learning frameworks for predicting the solubility of CO2 – N2 gas mixtures in brine: Implication for impure CO2 storage in saline aquifers, Journal of Contaminant Hydrology. 2025; 27: 4104660. https://doi.org/10.1016/j.jconhyd.2025.104660

[14] Chen Y., Xie Q., Yang Y., Mahani H., Niasar V., Nano structure of CO2-Brine-Kaolinite Interface: Implications for CO2 Geological Sequestration, Applied Clay Science. 2024; 254: 107391. https://doi.org/10.1016/j.clay.2024.107391

[15] Tang Y., Hu S., He Y., Wang Y., Wan X., Cui S., Long K., Experiment on CO2-brine-rock interaction during CO2 injection and storage in gas reservoirs with aquifer, Chemical Engineering Journal. 2021; 413: 127567. https://doi.org/10.1016/j.cej.2020.127567

[16] Mohammadian E., Hamidi H., Asadullah M., Azdarpour A., Motamedi S., Junin R., Measurement of CO2 Solubility in NaCl Brine Solutions at Different Temperatures and Pressures Using the Potentiometric Titration Method, J. Chem. Eng. Data. 2015; 60: 2042–2049. https://doi.org/10.1021/je501172d

[17] Gandomkar A., Torabi F., Nasriani H.R., Enick R.M., Maximising CO2 sequestration efficiency in deep saline aquifers through in-situ generation of CO2-in-brine foam incorporating novel CO2-soluble non-ionic surfactants, Chemical Engineering Journal. 2025; 521:166102. https://doi.org/10.1016/j.cej.2025.166102

[18] Allameh S., Shaker M., Milani A.H., Mn(II) complex based 3-hydroxynaphthoic acid: A recyclable catalyst in synthesis of novel quinoline-5-one derivatives, International Journal of Industrial Chemistry. 2021; 12. https://doi.org/10.47176/IJIC.12.2.2

[19] Wu X., Li J., Wang J., Cao L., Poly(butyl acrylate) gel prepared in supercritical CO2: an efficient recyclable oil-absorbent, International Journal of Industrial Chemistry. 2020; 11. https://doi.org/10.1007/s40090-020-00204-2

[20] Ren W., Li P., Performance of composite modified asphalt based on nano-organic montmorillonite and silica, International Journal of Industrial Chemistry. 2024; 15. https://doi.org/10.57647/j.ijic.2024.1501.08

[21] Khani M., Pordel M., Davoodnia A., TavasoliFarsheh A., Investigation of the effect of using ZnO/TiO2 nano particles on properties of the polyethylene terephthalate preform and beverage bottles, International Journal of Industrial Chemistry. 2022; 13. https://oiccpress.com/ijic/article/view/8246 (accessed December 8, 2025)

[22] Zarei E., Electrochemically assisted photocatalytic removal of m-cresol using TiO2 thin film-modified carbon sheet photoelectrode, International Journal of Industrial Chemistry. 2018; 9. https://doi.org/10.1007/s40090-018-0158-z

[23] Steele-MacInnis M., Capobianco R.M., Dilmore R., Goodman A., Guthrie G., Rimstidt J.D., Bodnar R.J., Volumetrics of CO2 Storage in Deep Saline Formations, Environ. Sci. Technol. 2013; 47 :79–86. https://doi.org/10.1021/es301598t

[24] Wang H., Li Y., Li C., Zhu H., Li Z., Wang L., Medina-Rodriguez B.X., Unveil the controls on CO2 diffusivity in saline brines for geological carbon storage, Geoenergy Science and Engineering. 2025; 244: 213483. https://doi.org/10.1016/j.geoen.2024.213483

[25] Rashidi S., Shariatipour S., Ahmadinia M., Synthesis of equilibrated geochemical systems using extended Debye-Huckel and Pitzer activity models for enhanced CO2 storage modelling, Gas Science and Engineering. 2026; 145: 205792. https://doi.org/10.1016/j.jgsce.2025.205792

[26] Tong D., Trusler J.P.M., Vega-Maza D., Solubility of CO2 in Aqueous Solutions of CaCl2 or MgCl2 and in a Synthetic Formation Brine at Temperatures up to 423 K and Pressures up to 40 MPa, J. Chem. Eng. Data. 2013; 58: 2116–2124. https://doi.org/10.1021/je400396s

[27] Mutailipu M., Song Y., Yao Q., Liu Y., Martin J.P. Trusler, Solubility and interfacial tension models for CO2–brine systems under CO2 geological storage conditions, Fuel . 2024; 35: 7129712. https://doi.org/10.1016/j.fuel.2023.129712

[28] Zubeir L.F., Romanos G.E., Weggemans W.M.A., Iliev B., Schubert T.J.S., Kroon M.C, Solubility and Diffusivity of CO2 in the Ionic Liquid 1-Butyl-3-methylimidazolium Tricyanomethanide within a Large Pressure Range (0.01 MPa to 10 MPa), J. Chem. Eng. Data 60 (2015) 1544–1562. https://doi.org/10.1021/je500765m

[29] Dehury R., Sangwai J.S., Pore-scale displacement dynamics of CO2 sequestration in subsurface aquifers: The role of brine salinity and wettability, Journal of Environmental Chemical Engineering 13 (2025) 117649. https://doi.org/10.1016/j.jece.2025.117649

[30] Bhattacherjee R., Pradhan S., Aichele C., Pashin J.C., Chakraborty G., Bikkina P., Predicting CO2 solubility in brines using density as a proxy for detailed compositional data: A data-driven modeling approach, Chemical Engineering Journal. 2025; 520: 166174. https://doi.org/10.1016/j.cej.2025.166174

[31] Liu K., Bian X.-Q., Chen J., Li J., Wang Y.-P., Predicting CO2 solubility in water and brines using advanced machine learning models, Geoenergy Science and Engineering. 2026; 257: 214234. https://doi.org/10.1016/j.geoen.2025.214234

[32] Wang Z., Small M.J., Karamalidis A.K., Multimodel Predictive System for Carbon Dioxide Solubility in Saline Formation Waters, Environ. Sci. Technol. 2013; 47: 1407–1415. https://doi.org/10.1021/es303842j

[33] Mohammadian E., Hamidi H., Asadullah M., Azdarpour A., Motamedi S., Junin R., Measurement of CO2 Solubility in NaCl Brine Solutions at Different Temperatures and Pressures Using the Potentiometric Titration Method, J. Chem. Eng. Data. 2015; 60: 2042–2049. https://doi.org/10.1021/je501172d

[34] Zhao H., Dilmore R., Allen D.E., Hedges S.W., Soong Y., Lvov S.N., Measurement and Modeling of CO2 Solubility in Natural and Synthetic Formation Brines for CO2 Sequestration, Environ. Sci. Technol. 2015; 49: 1972–1980. https://doi.org/10.1021/es505550a

[35] Gandomkar A., Torabi F., Nasriani H.R., Enick R.M., Maximising CO2 sequestration efficiency in deep saline aquifers through in-situ generation of CO2-in-brine foam incorporating novel CO2-soluble non-ionic surfactants, Chemical Engineering Journal. 2025; 521:166102. https://doi.org/10.1016/j.cej.2025.166102

[36] Bhattacherjee R., Botchway K., Pashin J.C., Chakraborty G., Bikkina P., Machine learning-based prediction of CO2 fugacity coefficients: Application to estimation of CO2 solubility in aqueous brines as a function of pressure, temperature, and salinity, International Journal of Greenhouse Gas Control. 2023; 128: 103971. https://doi.org/10.1016/j.ijggc.2023.103971

[37] Ratnakar R.R., Chaubey V., Dindoruk B., A novel computational strategy to estimate CO2 solubility in brine solutions for CCUS applications, Applied Energy. 2023; 342: 121134. https://doi.org/10.1016/j.apenergy.2023.121134

[38] Sun X., Wang Z., Li H., He H., Sun B., A simple model for the prediction of mutual solubility in CO2-brine system at geological conditions, Desalination. 20215; 04:114972. https://doi.org/10.1016/j.desal.2021.114972

[39] Hassanzadeh H., Pooladi-Darvish M., Keith D.W., Accelerating CO2 Dissolution in Saline Aquifers for Geological Storage — Mechanistic and Sensitivity Studies, Energy Fuels. 2009; 23: 3328–3336. https://doi.org/10.1021/ef900125m

[40] Turkson J.N., Md Yusof M.A., Olutoki J.O., Tackie-Otoo B.N., Adenutsi C.D., Fjelde I., Sokama-Neuyam Y.A., Darkwah-Owusu V., Integrating nature-inspired optimization techniques and machine learning for accurate CO2/brine interfacial tension estimation: Implications for CO2 sequestration and uncertainty analysis, Gas Science and Engineering. 2026; 145: 205796. https://doi.org/10.1016/j.jgsce.2025.205796

[41] Darkwah-Owusu V., Md Yusof M.A., Sokama-Neuyam Y.A., Fjelde I., Nguku A., Turkson J.N., Rosdi N., Vasudevan M., Alakbari F.S., Integrated geochemical modeling and experimental study of acid treatments for enhancing CO2 injectivity: Implications for geological CO2 storage, Geoenergy Science and Engineering. 2025; 249: 213793. https://doi.org/10.1016/j.geoen.2025.213793

[42] Tong D., Trusler J.P.M., Vega-Maza D., Solubility of CO2 in Aqueous Solutions of CaCl2 or MgCl2 and in a Synthetic Formation Brine at Temperatures up to 423 K and Pressures up to 40 MPa, J. Chem. Eng. Data .2013; 58: 2116–2124. https://doi.org/10.1021/je400396s

[43] Mohammadpour A., Mirzaei M., Azimi A., Ghomsheh S.M.T., Solubility and absorption rate of CO2 in MEA in the presence of graphene oxide nanoparticle and sodium dodecyl sulfate, International Journal of Industrial Chemistry. 2019; 10. https://doi.org/10.1007/s40090-019-0184-5

[44] Rathnaweera T.D., Ranjith P.G., Perera M.S.A., Haque A., Influence of CO2–Brine Co-injection on CO2 Storage Capacity Enhancement in Deep Saline Aquifers: An Experimental Study on Hawkesbury Sandstone Formation, Energy Fuels. 2016; 30 : 4229–4243. https://doi.org/10.1021/acs.energyfuels.6b00113

[45] Nowrouzi I., Mohammadi A.H., Manshad A.K., Water-oil interfacial tension (IFT) reduction and wettability alteration in surfactant flooding process using extracted saponin from Anabasis Setifera plant, Journal of Petroleum Science and Engineering 189 (2020) 106901. https://doi.org/10.1016/j.petrol.2019.106901

[46] Alotaibi M.B., Yousef A.A., The Role of Individual and Combined Ions in Waterflooding Carbonate Reservoirs: Electrokinetic Study, SPE Res Eval & Eng 20 (2016) 077–086. https://doi.org/10.2118/177983-PA

[47] Alshammari S., Abdel-Azeim S., Al-Yaseri A., Qasim A., The Influence of CH4 and CO2 on the Interfacial Tension of H2–Brine, Water–H2–Rock Wettability, and Their Implications on Geological Hydrogen Storage, Energy Fuels 38 (2024) 15834–15847. https://doi.org/10.1021/acs.energyfuels.4c02234

[48] Manshad A.K., Mobaraki M., Ali J.A., Abdulrahman A.F., Jaf P.T., Bahraminejad H., Akbari M., Biphasic interfacial functioning improvement using naturally derived Hop and Dill surfactants in carbonate reservoirs, Journal of Environmental Chemical Engineering 12 (2024) 112365. https://doi.org/10.1016/j.jece.2024.112365

[49] Alzobaidi S., Lotfollahi M., Kim I., Johnston K.P., DiCarlo D.A., Carbon Dioxide-in-Brine Foams at High Temperatures and Extreme Salinities Stabilized with Silica Nanoparticles, Energy Fuels 31 (2017) 10680–10690. https://doi.org/10.1021/acs.energyfuels.7b01814

[50] Akindipe D., Saraji S., Piri M., Carbonated Water Injection in Oil-Wet Carbonate Rock Samples: A Pore-Scale Experimental Investigation of the Effect of Brine Composition, Energy Fuels 36 (2022) 4847–4870. https://doi.org/10.1021/acs.energyfuels.2c00326

2228-5970 [https://doi.org/10.57647/j.ijic.2025.1604.19]